Supporting Information

Magnetic Assembly of Plasmonic Chiral Superstructures with Dynamic Chiroptical Responses

*Chaolumen Wu, Qingsong Fan, Zhiwei Li, Zuyang Ye, Yadong Yin**

Department of Chemistry, University of California, Riverside, CA 92521, USA

Simulation of magnetic flux density distribution from a cubic permanent magnet

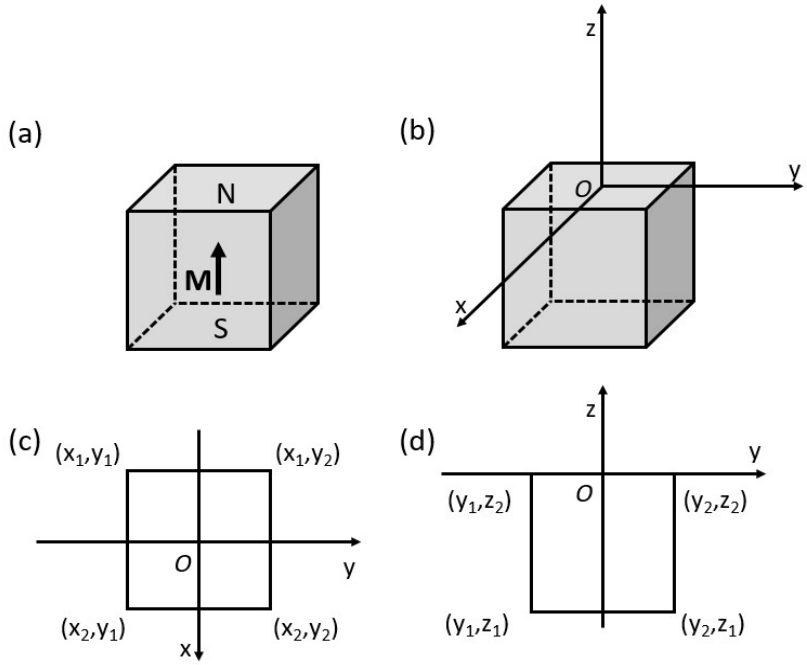

Scheme S1. A cubic permanent magnet. (a) geometry and polarization, (b) reference frame, (c) x-y plane view. (d) y-z plane view.

The field solution for a permanent magnet has been developed by Furlani[1,2] and is summarized here for convenience. For a cubic magnet magnetized along the z-axis direction, its magnetic field components are given by

$$B_x = \frac{\mu_0 M_e}{4\pi}\sum_{k=1}^{2}\sum_{m=1}^{2}(-1)^{k+m} ln\ln\left(F(x,y,z,x_m,y_1,y_2,z_k)\right) \quad Eq.S1.1$$

$$B_y = \frac{\mu_0 M_e}{4\pi}\sum_{k=1}^{2}\sum_{m=1}^{2}$$

$$Eq.S1.2 B_z = \frac{\mu_0 M_e}{4\pi}\sum_{k=1}^{2}\sum_{n=1}^{2}\sum_{m=1}^{2}(-1)^{k+n+m}\times\left[\frac{(x-x_n)(y-y_m)}{(z-z_k)}g(x,y,z;x_n,y_m,z_k)\right] \quad Eq.S1.$$

In the above equations, M_e is the magnetization of the element, (x_1, x_2), (y_1, y_2), and (z_1, z_2) are the locations of the corners and $\mu_0 = 4\pi \times 10^{-7}\ N/A^2$ is the magnetic permeability of free space.

The expressions for $F(x,y,z,x_m,y_1,y_2,z_k)$, $H(x,y,z,x_1,x_2,y_m,z_k)$ and $g(x,y,z;x_n,y_m,z_k)$ are as follows

$$F(x,y,z,x_m,y_1,y_2,z_k) = \frac{F_1(x,y,z,x_m,y_1,z_k)}{F_2(x,y,z,x_m,y_2,z_k)} \quad Eq.S1.4$$

where

$$F_1(x,y,z,x_m,y_1,z_k) = (y-y_1) + \left[(x-x_m)^2 + (y-y_1)^2 + (z-z_k)^2\right]^{\frac{1}{2}} \quad Eq.S1.5$$

$$F_2(x,y,z,x_m,y_2,z_k) = (y-y_2) + \left[(x-x_m)^2 + (y-y_2)^2 + (z-z_k)^2\right]^{\frac{1}{2}} \quad Eq.S1.6$$

and

$$H(x,y,z,x_1,x_2,y_m,z_k) = \frac{H_1(x,y,z,x_1,y_m,z_k)}{H_2(x,y,z,x_2,y_m,z_k)} \quad Eq.S1.7$$

where

$$H_1(x,y,z,x_1,y_m,z_k) = (x-x_1) + \left[(x-x_1)^2 + (y-y_m)^2 + (z-z_k)^2\right]^{\frac{1}{2}} \quad Eq.S1.8$$

$$H_2(x,y,z,x_2,y_m,z_k) = (x-x_2) + \left[(x-x_2)^2 + (y-y_m)^2 + (z-z_k)^2\right]^{\frac{1}{2}} \quad Eq.S1.9$$

and

$$g(x,y,z;x_n,y_m,z_k) = \frac{1}{\left[(x-x_n)^2 + (y-y_m)^2 + (z-z_k)^2\right]^{\frac{1}{2}}} \quad Eq.S1.10$$

In our simulation of the magnetic field distribution, the origin is chosen as the center of the top surface of the cubic magnet, except for some special cases when noted.

The parameters that we use in this simulation are summarized in the table:

Parameter	value	unit
Length of cubic permanent magnet	2	cm
Magnetization of the element, M_e	$1*10^6$	A/m

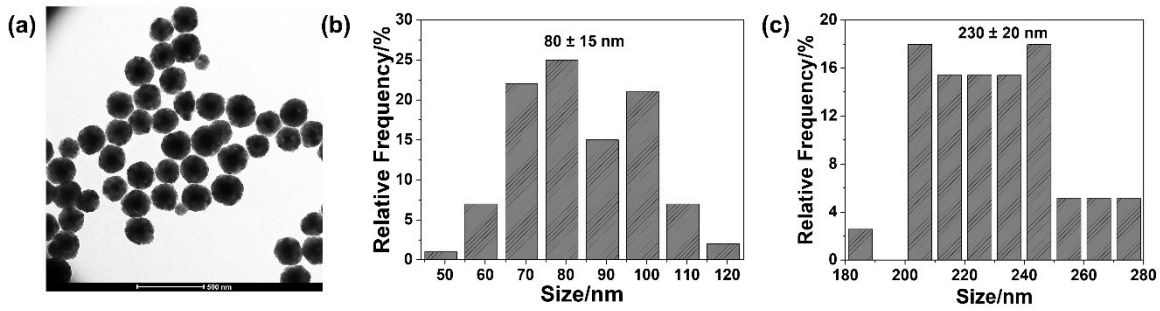

Figure S0. (a) Low magnification TEM image of $Ag@Fe_3O_4$ nanoparticles. Size distribution of (b) Ag core and (c) $Ag@Fe_3O_4$ nanoparticles.

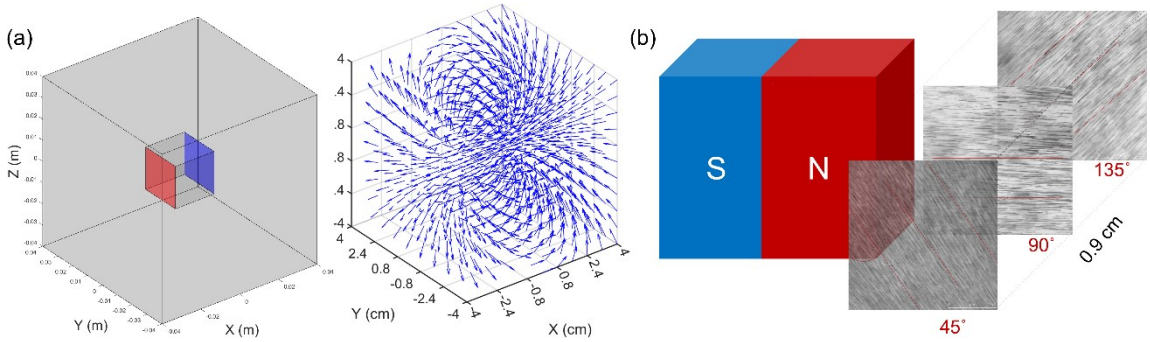

Figure S1. (a) Simulation of magnetic field distribution of a cubic permanent magnet (2 cm × 2 cm). (b) Chiral arrangement of the one-dimensional nanochains assembled under the chiral magnetic field.

As shown in Figure S1b, the $Ag@Fe_3O_4$ nanoparticle assembly under the chiral magnetic field was fixed in a photocurable polymer, forming a chiral film. The optical microscopic images clearly showed the formation of one-dimensional nanochains of nanoparticles caused by the magnetic dipole-dipole interaction. Simultaneously, the chiral magnetic field drove the nanochains into chiral arrangements, forming hierarchical chiral superstructures. The nanochains orientation varied from 45 to 135˚ within 0.9 cm from the left to right side of the magnet, showing the helical arrangement of the nanochains.

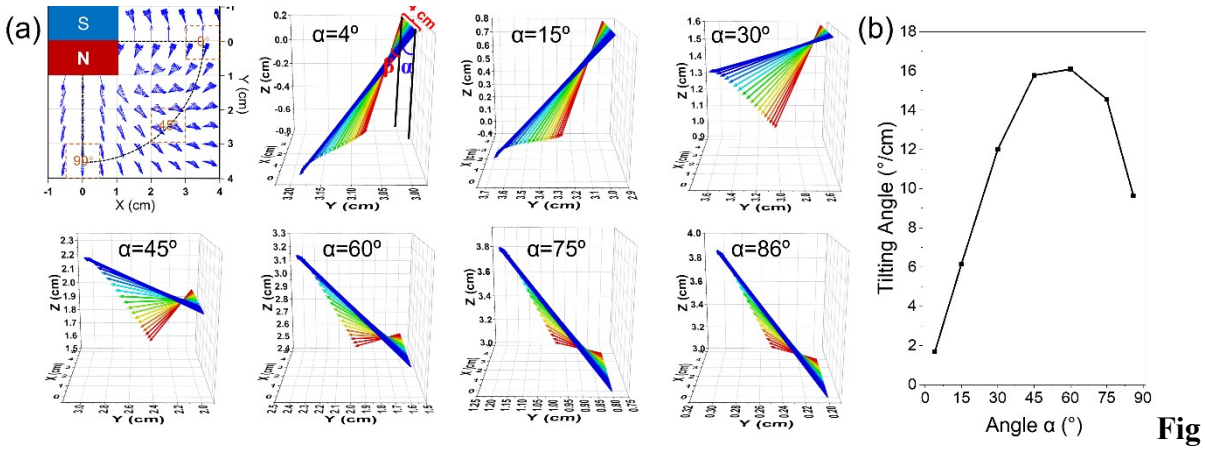

Figure S2. (a) Simulation of tilting angles of magnetic field vectors under different α from 4 to 86°. (b) The relationship between α and the tilted angle of the magnetic field vector.

The tilting angle of the magnetic field vector is defined as the difference between the initial intersection angle (γ) and the final intersection angle (δ) of the magnet field vector and Z-axis, and the initial and final position is along the X-axis, and the distance between them is 4 cm. Then the tilting angle per cm equals to (γ-δ)/4 cm, and it represents the helix angle of the chiral nanostructures.

We calculated the tilted angle per cm at varying α from 4 to 86°, and the value was first increased and then decreased (Figure S2b).

Pitch (P) of a chiral nanostructure is defined by the following equation:

$$P=\pi D\tan(90-\theta),$$

P: Pitch
D: Diameter of helical circle
θ: helix angle

Thus, it is clear that the P decreases with the increasing of θ, indicating the increase of the chirality asymmetry, which increases the CD intensity.

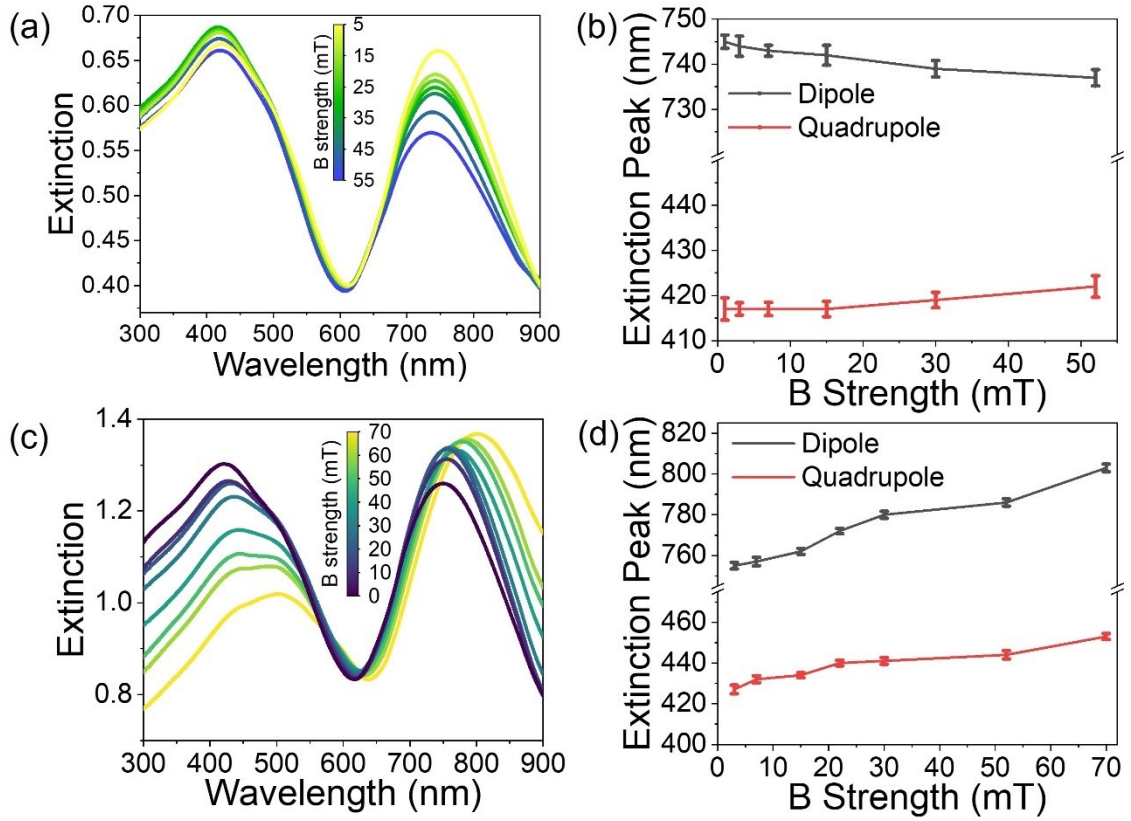

Figure S3. (a, c) Extinction spectra and (b, d) the corresponding dipole and quadrupole peak shifts of the Ag@Fe_3O_4 nanoparticle assembly under different strengths of B_x and B_y, respectively.

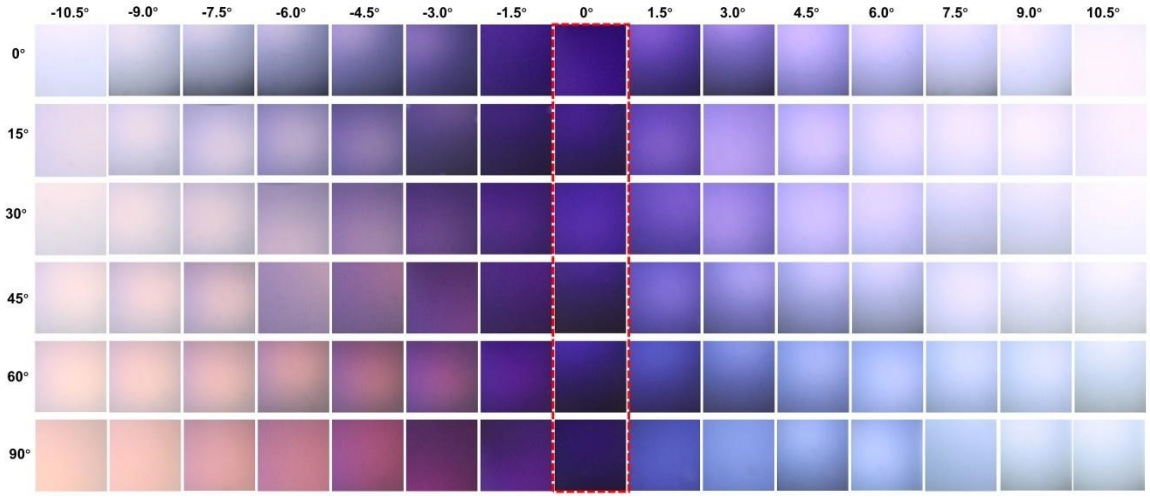

Figure S4. ORD images of Ag@Fe_3O_4 nanoparticle dispersion under varying α from 0 to 90º as β varied from -10.5 to 10.5º.

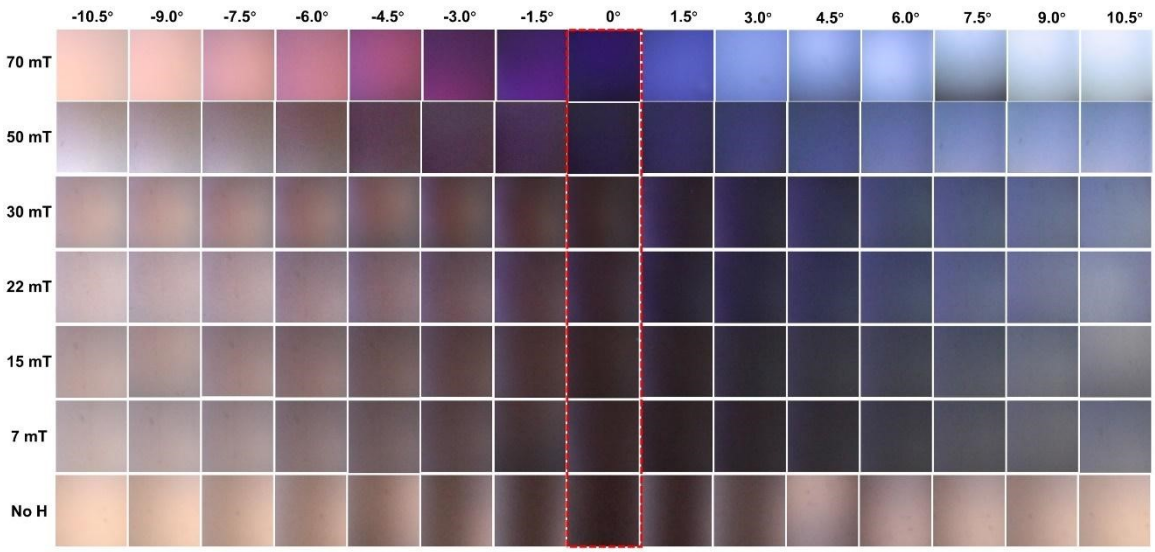

Figure S5. ORD images of $Ag@Fe_3O_4$ nanoparticle dispersion under B_x with different strengths as β varied from -10.5 to 10.5º.

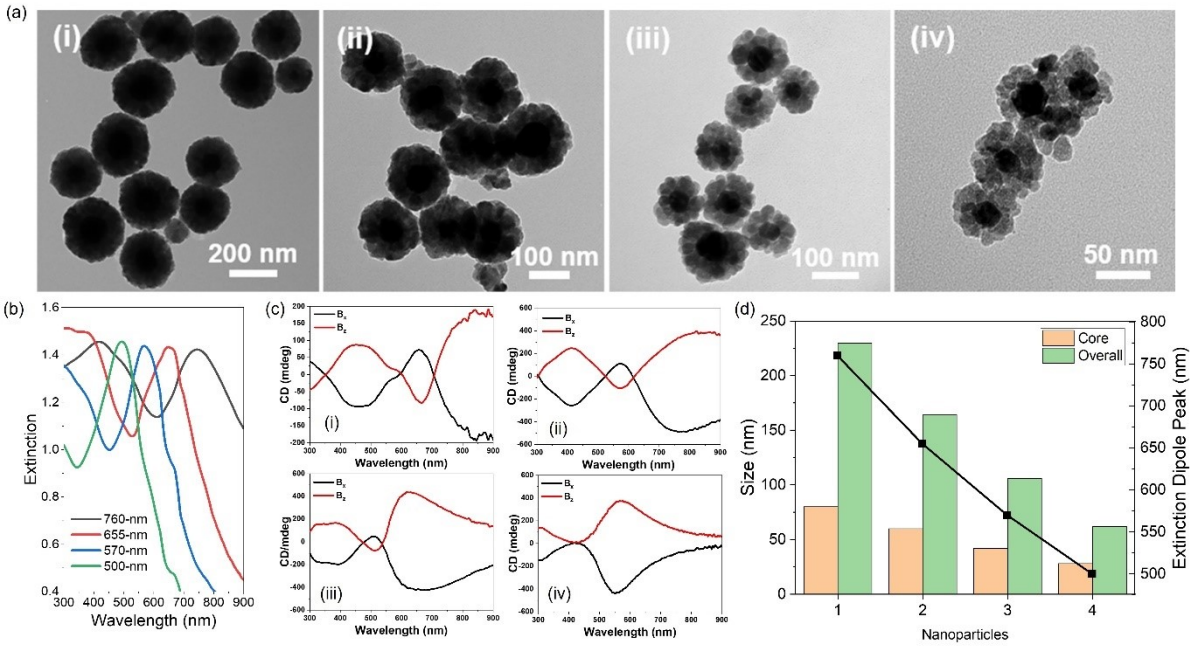

Figure S6. (a) TEM images of $Ag@Fe_3O_4$ with different extinction dipole peaks: (i) 760 nm, (ii) 655 nm, (iii) 570 nm, (iv) 500 nm, and (b) the corresponding extinction spectra without magnet, and CD spectra (c) under B_x, and B_z. (d) The relationship between the $Ag@Fe_3O_4$ sizes and the extinction dipole peaks.

With the increase of both Ag core size and Fe_3O_4 shell thickness, the extinction peak of the nanoparticles are gradually red shifted due to the increase in both Ag nanoparticle size and the surrounding refractive index from the shell. This plasmonic resonance red shifts was trasfered to the chiral optical properties. Figure S6c shows the red shift on both dipole and quadrupole CD peaks with the increase of the nanoparticle sizes.

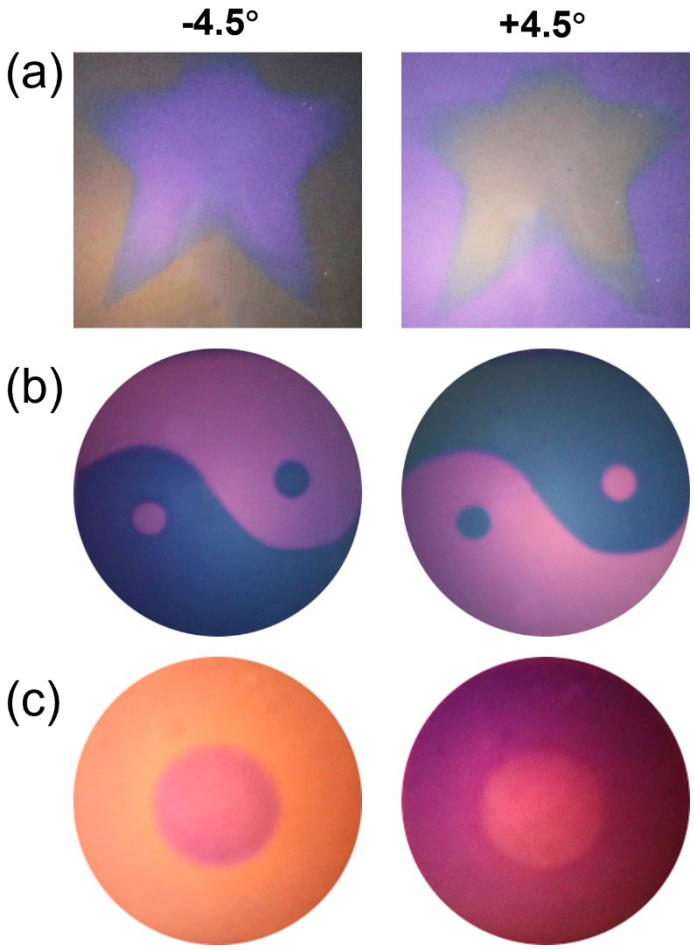

Figure S7. ORD images of the chiral films from the assembly of (a) 655-nm, (b) 570-nm, (c) 500-nm nanoparticles with different patterns under β=±4.5º.

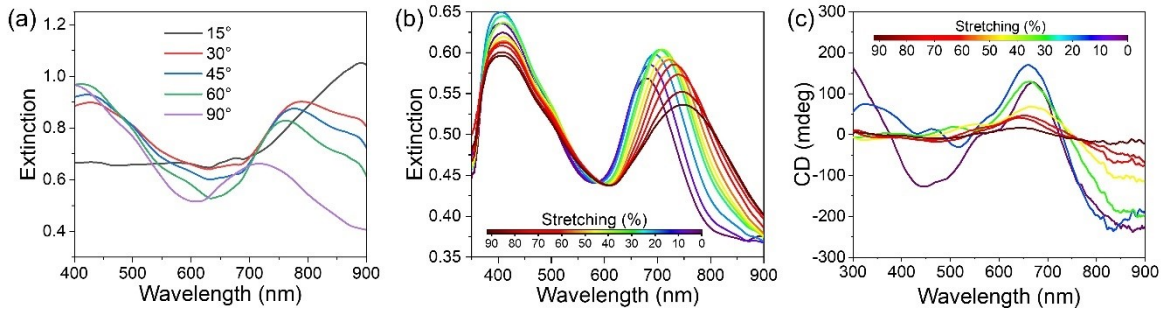

Figure S8. (a) Extinction spectra of the chiral film with tilting angle varied from 15º to 90º. (b) Extinction and (c) CD spectra of the chiral film under stress as tilting angle fixed as 90º.

Reference:

1. Furlani, E.P. (2001). Permanent magnet and electromechanical devices: materials, analysis, and applications (Academic press).
2. Xue, X., and Furlani, E.P. (2015). Analysis of the dynamics of magnetic core–shell nanoparticles and self-assembly of crystalline superstructures in gradient fields. The Journal of Physical Chemistry C *119*, 5714-5726.